The International Journal of Advanced Manufacturing Technology (2018) 99:1953–1966
https://doi.org/10.1007/s00170-018-2567-8

ORIGINAL ARTICLE

Investigation on the influence of interference fit on the static and dynamic characteristics of spindle system

Guanghui Liu[1] · Jun Hong[1] · Wenwu Wu[2] · Yanhui Sun[1]

Received: 17 February 2018 / Accepted: 13 August 2018 / Published online: 30 August 2018

Abstract

The performance of high-speed and high-precision machine tool spindle is quite sensitive to the variation of system parameters. How to accurately predict the influences of key parameters on spindle characteristics is important for designers to achieve required machining accuracy. In the assembly of spindle system, the interference fit, which is always used to connect bearing and shaft, affects the performances of spindle system directly. Therefore, the quantitative investigation on the effects of interference fit on spindle characteristics are of great practical significance. In this paper, the effect mechanism of interference fit on spindle bearing system is explored and used to modify the analytical spindle bearing model. Firstly, the internal geometric relationships among the assembly bearing parts and shaft is analyzed under the influence of assembly deformation and centrifugal expansion. Then, the static and dynamic characteristics of spindle bearing system, including the bearing stiffness, maximum loosing speed, spindle stiffness as well as modal characteristics, are predicted under different interference fit values based on the modified spindle bearing model. The results show that the interference fit will stiffen the bearing and spindle system and result in obvious increments on bearing stiffness, spindle stiffness as well as the natural frequencies. A specially designed spindle test rig is built to verify the simulation results, and the variation of spindle stiffness and natural frequencies are measured under different interference fit values. The maximum error of the system natural frequencies between the analytical results and the experimental data is 7.36%, which confirmed the accuracy of the proposed analytical model.

Keywords Interference fit · Spindle bearing model · Assembly parameter · Loosing speed · Static and dynamic characteristics

1 Introduction

Spindle system is one of the key components of machine tools, which will determine the machining quality directly. With the increasing requirements for machining performance, the spindle system is developing towards the direction of high speed and high precision. However, the static and dynamic characteristics of spindle system are greatly influenced by the variation of system parameters. The accuracy of performance prediction of the spindle system is essential and of great practical significance.

The research on the spindle bearing system has been widely conducted during the past several decades. High-speed and high-precision spindle and bearing techniques are receiving more and more attentions [1, 2]. In this process, some general dynamic spindle bearing models are built to predict and improve the system characteristics. The establishment of analytical model of spindle system is generally based on the rotor dynamics combined with linear or nonlinear bearing models. Researchers [3, 4] had established some spindle models to predict the performances of spindle system in the design stage. With the development of high-speed machine tool spindles [5, 6], the effects of centrifugal loading were gradually taken into consideration. Cao [7, 8] built a spindle-bearing model considering the shaft, bearing, and housing assembly. The spindle modal characteristics were analyzed and verified by experiments. Jiang [9] presented a dynamic model based on the traditional transfer matrix method coupled with a nonlinear rolling bearing model to study the effects of the extended

✉ Jun Hong
jhong@mail.xjtu.edu.cn

[1] Key Laboratory for Modern Design & Rotor-Bearing System, Xi'an Jiaotong University, Xi'an 710049, China

[2] Key Laboratory of NC Machine Tools and Integrated Manufacturing Equipment of the Ministry of Education & Key Laboratory of Manufacturing Equipment of Shaanxi Province, Xi'an University of Technology, Xi'an 710048, China

structure parameters on the vibration behavior of a high-speed motorized spindle-bearing system. Frequency response function (FRF) is always used to reflect the dynamic characteristics of spindle system. A high-speed dynamic spindle model was described by Shaik [10], and the spindle FRFs were calculated and verified by experiments. Similarly, the static stiffness and FRFs of a spindle system under different bearing preload mechanisms was calculated by Cao [11] using both mathematical model and experimental method under various bearing preload conditions. With the increase of spindle accuracy, the influences of some subassemblies on the spindle system have been gradually taken into consideration. The influences of the spindle-holder-tool joints were fully investigated and coupled into the spindle bearing model [12–17] to accurately predict the dynamic responses of the spindle system. Besides, the effects of spindle housing and machine frame on system dynamic characteristics were also considered in the modeling of spindle bearing system [8, 18]. Some coupling models further include the thermal or electromagnetic influences on spindle system. Zivkovic [19] presented a thermo-mechanical model to investigate the influence of bearing friction heat on spindle machining accuracy. Moreover, much more research was conducted considering the heat generation of both bearings and the built-in motor [20–25]. For high-precision spindles, the unbalanced electromagnetic force due to nonuniform air gap between the stator and the rotor was further studied and coupled into the analytical spindle model [26]. The general methods of modeling spindle system have been investigated extensively. However, the influences of assembling condition of bearing and shaft on spindle performance are not considered in current literature.

In machine tool spindle system, angular contact ball bearing is most commonly used for its excellent high-speed performance and the good loading capacity both in radial and axial directions. Some researchers have confirmed that the performances of bearing have great influence on spindle system [27, 28]. A lot of bearing fundamental investigations have been conducted based on the models developed by Jones [29] and Harris [30]. Xi [31] presented the influences of bearing radial clearance on the system dynamic responses and concluded that the natural frequencies of the spindle system increased greatly with the decrease of the radial clearance of the floating displacement bearing. Yan [32] investigated the thermal characteristics of the spindle bearing system based on the thermal network method, and the influence of bearing interference fit was taken into consideration in the calculation of bearing heat generation. Cao [33] described the effects of bearing clearance on bearing vibration, contact forces, and reaction moments based on a combined finite element and discrete element method dynamic gear-shaft model. A bearing stiffness model was established by Zhang [34] considering the influence of inner ring interference fit value and rotating speed. Two different types of preload mechanisms of bearing were discussed in detail, and the results were validated by comparing with other literature and experiments.

The current literature has studied the general modeling of spindle bearing system and verified the great influences of parameters, such as preload, centrifugal force, and gyroscopic effects, on spindle static and dynamic characteristics. However, the influences of interference fit, which is always introduced in the assembly of bearing and shaft, are not investigated systematically, especially in the analysis of static and dynamic characteristics of a whole spindle system.

The internal contact condition of the bearing as well as the matching surface between bearing and shaft will be greatly affected by the initial values of interference fit, which is crucial for high-speed and high-precision bearing and spindle systems due to its high sensitivity to system parameter variations. The precision of the bearing and spindle will reduce seriously if the interference fit values are designed unsuitably. Besides, the bearing heat generation, spindle vibration, and noise will also increase rapidly with inappropriate bearing fit values. Therefore, it is necessary to establish accurate analytical models to investigate the influences of interference fit on bearing and spindle system quantitatively.

The outline of the paper is as follows. Section 2 contains the modeling of bearing and spindle system considering the effects of interference fit, which is the magnitude of interference value between bearing inner ring and the mating shaft. Based on the Harris's quasi-static bearing model, the interference-induced change of contact conditions and relative positions among bearing assemblies are further reestablished. The bearing stiffness under different interference fit values could be predicted. Moreover, a spindle bearing model is presented and the influences of bearing interference fit are further coupled into the spindle system. In Sect. 3, the variation of bearing and spindle static and dynamic characteristics, including the bearing stiffness, bearing-shaft losing speed, spindle stiffness, natural frequencies, and frequency response functions, are predicted with the changing of bearing interference fit values based on the proposed model. In order to verify the simulation results of the analytical model, a specially designed spindle test rig is described in Sect. 4 to measure the spindle static stiffness and modal characteristics. The overall conclusions are given in Sect. 5.

2 Dynamic model of the spindle-bearing system considering interference fit

The interference fit will result in an extra elastic deformation on shaft and bearing parts. Then, the internal relationships among the assembly parts will change with the variation of the deformations, as shown in Fig.1a, b, which will have a great effect on the bearing stiffness as well as the spindle static and dynamic characteristics.

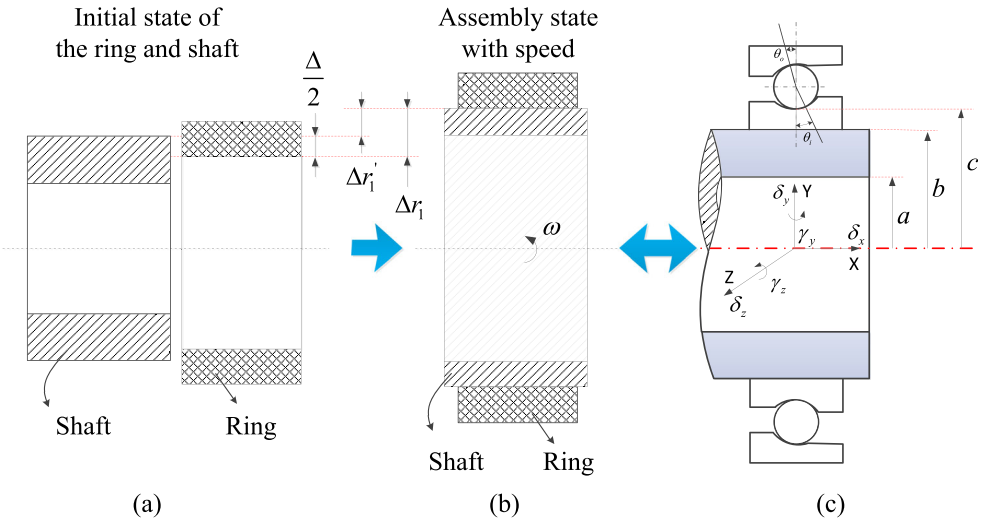

Fig. 1 Assembly relationship between bearing ring and shaft

In this section, considering the assembly elastic deformations and centrifugal expansion of the bearing inner ring and shaft, a theoretical model of the interference fit is established and then coupled into the spindle-bearing system to ascertain its effect on the bearing model.

2.1 Interference fit model of the bearing ring and shaft

The value of the interference fit should be designed properly to make sure the connection reliability between the bearing inner ring and the shaft under working conditions. Based on the theory of the thermo-elasticity and the mechanical features of the parts, the bearing inner ring is assumed as a thin ring for the calculation of radial deformation, while the shaft could be assumed as an infinite cylinder.

The thickness and width of the bearing inner ring are small compared with its diameter. So, the calculation of ring radial deformation is a two-dimensional plane stress problem. The equilibrium equation can be written as

$$\frac{\mathrm{d}\sigma_r}{\mathrm{d}r}+\frac{\sigma_r-\sigma_\theta}{r}+\rho\omega^2 r=0 \tag{1}$$

The geometric equations are

$$\begin{cases}\varepsilon_r=\dfrac{\mathrm{d}u}{\mathrm{d}r}\\ \varepsilon_\theta=\dfrac{u}{r}\end{cases} \tag{2}$$

The stress-strain equations are

$$\begin{cases}\sigma_r=\dfrac{E}{1-\nu^2}\left[\varepsilon_r+\nu\varepsilon_\theta\right]\\ \sigma_\theta=\dfrac{E}{1-\nu^2}\left[\varepsilon_\theta+\nu\varepsilon_r\right]\end{cases} \tag{3}$$

where E is the elasticity modulus, and ν is the poisson ratio.

Then, the differential relation between ring radial deformation u and radial position r can be derived as

$$\frac{\mathrm{d}^2u}{\mathrm{d}r^2}+\frac{1}{r}\frac{\mathrm{d}u}{\mathrm{d}r}-\frac{u}{r^2}=-\frac{\rho\omega^2 r(1-\nu^2)}{E} \tag{4}$$

where ρ is the material density, and ω is the angular velocity of the bearing inner ring.

The radial deformation of the bearing inner ring $u_{ring}(r)$ could be obtained by solving the differential equation and shown as

$$u_{ring}(r)=C_1 r+\frac{C_2}{r}-\frac{\rho\omega^2 r^3(1-\nu^2)}{8E} \tag{5}$$

where C_1, C_2 are the constants related to the boundary conditions.

Assume that P is the contact pressure between the bearing inner ring and shaft, hence the boundary conditions could be determined as

$$\begin{cases}r=b, & \sigma_r=-P\\ r=c, & \sigma_r=0\end{cases} \tag{6}$$

where the b and c are the related ring inner and outer radii, as shown in Fig. 1c. Then, the constants C_1 and C_2 can be formulated as

$$\begin{cases}C_1=\dfrac{(1-\nu)}{8E\left(c^2-b^2\right)}\left(8Pb^2+(3+\nu)\rho\omega^2\left(c^4-b^4\right)\right)\\ C_2=\dfrac{(1+\nu)c^2b^2}{8E\left(c^2-b^2\right)}\left(8P+(3+\nu)\rho\omega^2\left(c^2-b^2\right)\right)\end{cases} \tag{7}$$

As for the shaft, the solving of its radial deformation can be recognized as a plane strain problem. The shaft radial deformation can be easily obtained on the basis of the ring deformation result by replacing E, $\alpha$and ν in Eq. (5) with $\frac{E}{1-\nu^2}$,(1 +

$\nu)\alpha$ and $\frac{\nu}{1-\nu}$, respectively. The radial deformation of the shaft $u_{shaft}(r)$ could be expressed as

$$u_{shaft}(r) = C_3 r + \frac{C_4}{r} - \frac{\rho\omega^2 r^3(1-2\nu)(1+\nu)}{8E(1-\nu)} \tag{8}$$

Similarly, the boundary conditions are

$$\begin{cases} r = b, & \sigma_r = -P \\ r = a, & \sigma_r = 0 \end{cases} \tag{9}$$

Then, the constants C_3 and C_4 can be determined as

$$\begin{cases} C_3 = \dfrac{(1+\nu)(1-2\nu)}{8E\left(b^2-a^2\right)}\left(-8Pb^2 + \dfrac{3-2\nu}{1-\nu}\rho\omega^2\left(b^4-a^4\right)\right) \\ C_4 = \dfrac{(1+\nu)a^2b^2}{8E\left(b^2-a^2\right)}\left(-8P + \dfrac{3-2\nu}{1-\nu}\rho\omega^2\left(b^2-a^2\right)\right) \end{cases} \tag{10}$$

Thence, the radial deformation of the bearing inner ring and the shaft can be expressed as a function of the contact pressure P and their radial position r.

According to the deformation compatibility condition, as shown in Fig. 2, the relationship between the bearing and shaft radial deformations should be

$$u_{ring}(b) - u_{shaft}(b) = \Delta/2 \tag{11}$$

where$\Delta$is the value of the interference fit.

The linear equations can be expressed as $\mathbf{A}\cdot\mathbf{M} = \mathbf{B}$ by adopting simultaneous Eqs. (5), (7), (8), (10), and (11), where

$$\mathbf{M} = \left[P, u_{ring}(b), u_{shaft}(b)\right]^T \tag{12}$$

A and **B** are constant matrices which could be obtained by transposition.

Then, the parametric vector **M** is determined by calculating the equation group and the deformations of the bearing inner ring and shaft at any radial position could be obtained afterwards.

2.2 Bearing model with the influence of interference fit

Based on the Jones' bearing model, a 5-DOF quisa-dynamic model is established considering both the centrifugal forces and gyroscopic moments from the rolling elements of the bearing. In this model, the Hertizian contact theory is used to compute the contact deformation between bearing balls and bearing rings.

In this paper, the influence of interference fit is considered in the bearing model. The radial deformation of the bearing inner ring $u_{ring}(c)$, which could be calculated by Eq. (5), is actually the expansion of the contact diameter of bearing inner raceway d_i, which will further affect the initial bearing contact angle and relative displacements of bearing inner and outer rings. The relative motion of the bearing inner ring with respect to the outer ring is used in the model, so the curvature center of the outer ring groove can be assumed as being fixed. The unloaded currvature centers of bearing rings are colinear with the initial position of ball center. However, the loaded ring curvature centers are noncolinear with the ball center position due to the unequal change of the bearing inner and outer contact angles. The geometry of an angular contact ball bearing as well as the internal geometric relationships among bearing parts under a specific bearing load are shown in Fig. 2.

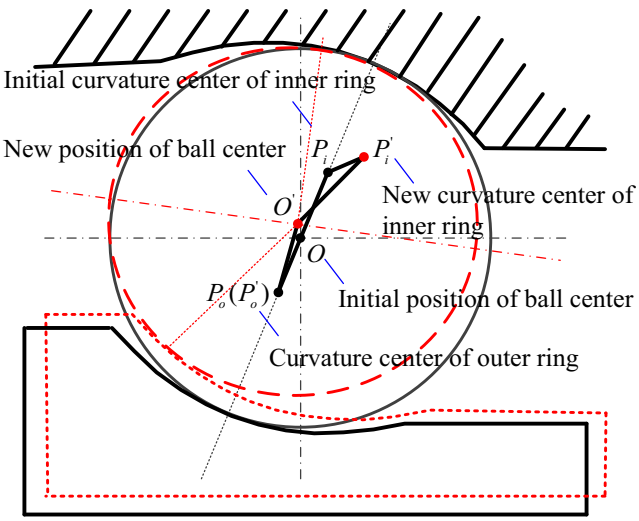

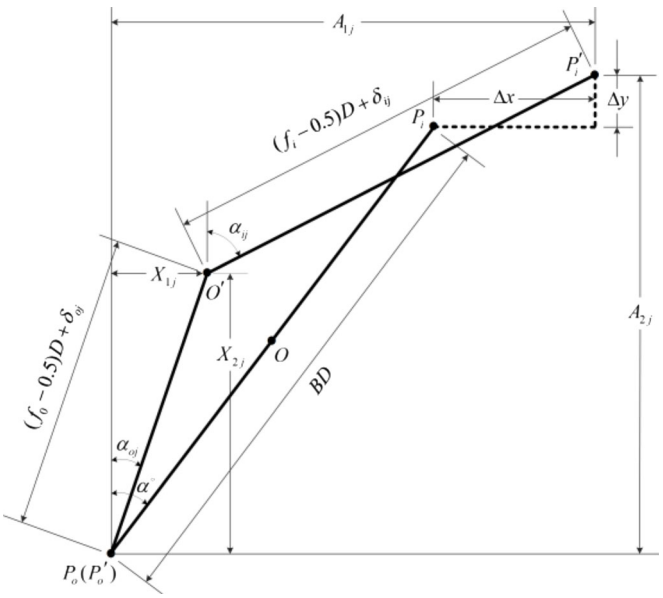

Fig. 2 Schematic diagram of bearing internal relationships

The initial contact angle of the bearing under the influence of interference fit could be expressed as

$$\alpha^o = arcos\left[1-\frac{d_o-\left(d_i+2u_{ring}(c)\right)-2D}{2(r_o+r_i-D)}\right] \tag{13}$$

where d_i,d_o are the inner and outer raceway contact diameters;r_i,$r_o$are the inner and outer raceway groove curvature radii;$D$is the diameter of bearing ball. According to the Pythagorean theorem, the displacement equations are

$$\begin{cases} A_{1j}-X_{1j})^2 \left(+ (A_{2j}-X_{2j}\right)^2-\left[(f_i-0.5)D+\delta_{ij}\right]^2 = 0 \\ X_{1j}^2+X_{2j}^2-\left[(f_o-0.5)D+\delta_{oj}\right]^2 = 0 \end{cases} \tag{14}$$

where

$$\begin{cases} A_{1j} = BD\sin\alpha^{^\circ}+\Delta x \\ A_{2j} = BD\sin\alpha^{^\circ}+\Delta y \end{cases} \tag{15}$$

$$\begin{cases} \Delta x = \Delta\delta_x-\Delta\gamma_z R_i\cos\varphi_k+\Delta\gamma_y R_i\sin\varphi_k \\ \Delta y = \Delta\delta_y\cos\varphi_k+\Delta\delta_z\sin\varphi_k \end{cases} \tag{16}$$

The $\Delta\delta_x$, $\Delta\delta_y$, $\Delta\delta_z$, $\Delta\gamma_y$, and$\Delta\gamma_z$ are the relative displacements between the inner ring and the outer ring.

The contact forces between the inner ring and the balls, and the outer ring and the balls, can be derived by analyzing the forces acting on the bearing rings, as well as considering the centrifugal force and gyroscopic moment. The equilibrium of the bearing ball could be expressed as

$$\begin{cases} \mathrm{Q}_{oj}\cos\alpha_{oj}-\frac{M_{gk}}{D}\sin\alpha_{oj}-\mathrm{Q}_{ij}\cos\alpha_{ij}+\frac{M_{gk}}{D}\sin\alpha_{ij}-F_{ck} = 0 \\ \mathrm{Q}_{oj}\sin\alpha_{oj}+\frac{M_{gk}}{D}\cos\alpha_{oj}-\mathrm{Q}_{ij}\sin\alpha_{ij}-\frac{M_{gk}}{D}\cos\alpha_{ij} = 0 \end{cases} \tag{17}$$

where Q_{ij} and Q_{oj} are the contact forces of the j^{th} bearing ball with inner and outer ring, respectively; $\alpha_{ij}$and α_{oj} are the contact angles between bearing ball with inner and outer rings, respectively. M_{gk} and F_{ck} are the gyroscopic moment and centrifugal force on the bearing ball, and the detailed expressions and derivations could be found in [35].

The relationship between the forces acting on the bearing rings and the relative displacements could be established by analyzing the global equilibrium of bearing rings. The forces acting on the bearing inner ring could be expressed as

$$\begin{cases} F_{xi} = \sum_{j=1}^{N}\left(\mathrm{Q}_{ij}\sin\alpha_{ij}+\frac{M_{gk}}{D}\cos\alpha_{ij}\right) \\ F_{yi} = \sum_{j=1}^{N}\left(\mathrm{Q}_{ij}\cos\alpha_{ij}-\frac{M_{gk}}{D}\sin\alpha_{ij}\right)\cos\psi_j \\ F_{zi} = \sum_{j=1}^{N}\left(\mathrm{Q}_{ij}\cos\alpha_{ij}-\frac{M_{gk}}{D}\sin\alpha_{ij}\right)\sin\psi_j \\ M_{yi} = \sum_{j=1}^{N}\left[r_{ic}\left(\mathrm{Q}_{ij}\cos\alpha_{ij}+\frac{M_{gk}}{D}\cos\alpha_{ij}\right)-f_i M_{gk}\right]\sin\psi_j \\ M_{zi} = -\sum_{j=1}^{N}\left[r_{ic}\left(\mathrm{Q}_{ij}\cos\alpha_{ij}+\frac{M_{gk}}{D}\cos\alpha_{ij}\right)-f_i M_{gk}\right]\cos\psi_j \end{cases} \tag{18}$$

where $\psi_j = 2\pi j/N$is the position angle of the j^{th} bearing ball.

$$r_{ic} = D_m/2+(r_i/D-0.5)D\cos\alpha^o \tag{19}$$

$D_m$is the pitch diameter of the bearing measured from the ball center.

Then, the stiffness matrix of the bearing can be obtained by finding the derivatives of forces with respect to displacement.

2.3 Dynamic model of spindle-bearing system

The beam element is still a good choice to model the motion of axis-symmetry structures for its high precision and ease to program. In this model, the Timoshenko beam element is used to establish the shaft model. Five degrees of freedom are included for each node of the elements, including three translational degrees of freedom and two rotational degrees of freedom. The torsional motion of the shaft is neglected.

The nondamping equation of motion for the beam element could be expressed as follows:

$$[M_s]\left\{\ddot{x}\right\}+\Omega[G_s]\left\{\dot{x}\right\}+\left([K_s]+[K_F]-\Omega^2[M_c]\right)\{x\} = \{F_s\} \tag{20}$$

where $[M_s]$ is the mass matrix, $[M_c]$ is the additional mass matrix due to the centrifugal effect; $[G_s]$ is the antisymmetric gyroscopic matrix; $[K_s]$ is the stiffness matrix, $[K_F]$ is the additional stiffness matrix due to the axial force; $[F_s]$ is the external force vector. Ω is the shaft rotational speed.

The attachments of the spindle system, such as the spacer, locknut, are modeled as the rigid disks [35]. By coupling the models of different kinds of parts, including the nonlinear bearing model considering the influence of interference fit, the analytical model of the spindle system can be expressed as

$$[M]\left\{\ddot{x}\right\}+[C]\left\{\dot{x}\right\}+[K]\{x\} = \{F(t)\} \tag{21}$$

The Newton-Raphson method is used to solve the equation of motions. Based on the established model, the analysis of spindle dynamic characteristics can be conducted, including the calculation of bearing stiffness, spindle system static stiffness, modal characteristics, and system frequency response functions.

3 Simulation results and discussion

Based on the derivations of the spindle bearing analytical model in the preceding section, the influences of the bearing interference fit values on the bearing and spindle characteristics could be simulated. In this section, the variation of bearing stiffness, static stiffness of the spindle system as well as the natural frequencies will be calculated under different conditions.

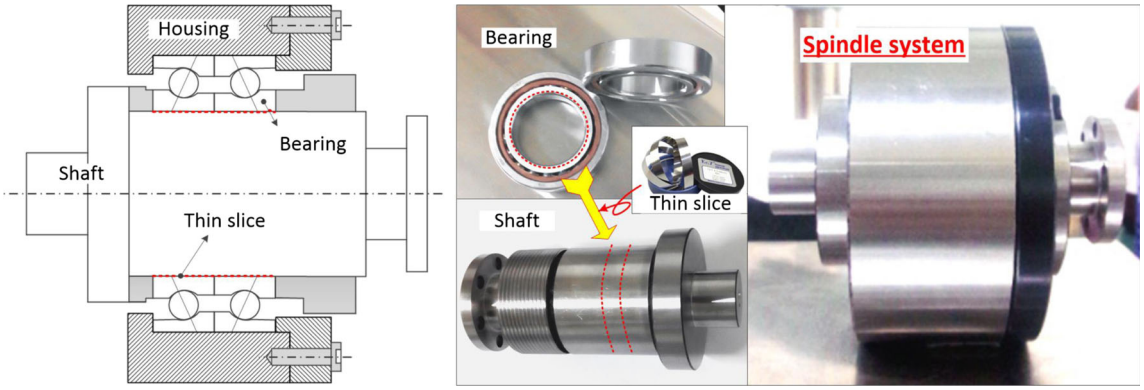

Fig. 3 The structure and the assemble sketch of spindle system

A spindle system supported by a back-to-back group bearing is chosen as the study case, as shown in Fig. 3. The supporting bearing is angular contact ball bearing and the detailed parameters are given in Table 1. The bearings are mounted by fix-position preload mechanism and are axially fixed by locknut. In the process of bearing assembly, thin slices are used between the shaft and bearing inner rings to adjust the value of interference fit, as shown in Fig. 3.

3.1 Influence of interference fit on bearing stiffness

3.1.1 Influence of interference fit on bearing stiffness under different preloads

The variation of bearing radial stiffness are shown on Fig. 4 with the changing of bearing preloads. In order to investigate the influence of interference fit between bearing inner ring and shaft, different values are specified for the comparison with the case without considering the influence of interference fit.

The results show that the bearing stiffness rise nonlinearly with the increase of bearing preload. This phenomenon has been investigated by many researchers. However, if the interference fit is taken into consideration, there will be an obvious increase in the bearing stiffness. Besides, the influence of interference fit on bearing stiffness is much more prominent in the low-preload cases. The reason could be found by analyzing the influence mechanism of the interference fit on bearing stiffness. According to the derivation in the preceding section, the interference fit affects the bearing stiffness through modifying the interior contact condition of bearing subassemblies, which is similar to the influence of the bearing preload. For the light preload bearing, the weighting of bearing interference fit is comparable to the weighting of bearing preload, so the bearing stiffness has a great rise with the increasing of bearing interference fit. However, for the high-preload cases, even though the preload dominates the increment of bearing stiffness, the effects of interference fit are still remarkable and nonnegligible. It is known that the light or extra light bearing preloads are usually used in the spindles with high rotating speed, which is just in line with the request of the high efficiency and precision machine tools. So, the interference fit must be considered in order to predict the bearing stiffness accurately.

3.1.2 Bearing stiffness variation under different interference fit values

Much more detailed relationship between bearing stiffness and bearing interference fits are investigated by continuously changing the values of interference fit between bearing inner ring and shaft. The variation of the bearing stiffness are shown in Fig. 5. With the increasing of bearing interference fit, the bearing stiffness shows a nonlinear rise swiftly.

Table 1 B7008CD angular contact ball bearing parameters

Parameter	Value	Parameter	Value
Inner diameter (mm)	40	Inner race contact diameter (mm)	46.058
Outer diameter (mm)	68	Outer race contact diameter (mm)	61.957
Ball diameter (mm)	7.938	Number of balls	18
Groove curvature radius of inner race (mm)	4.31	Groove curvature radius of outer race (mm)	4.158
Bearing width (mm)	15	Contact angle (°)	15

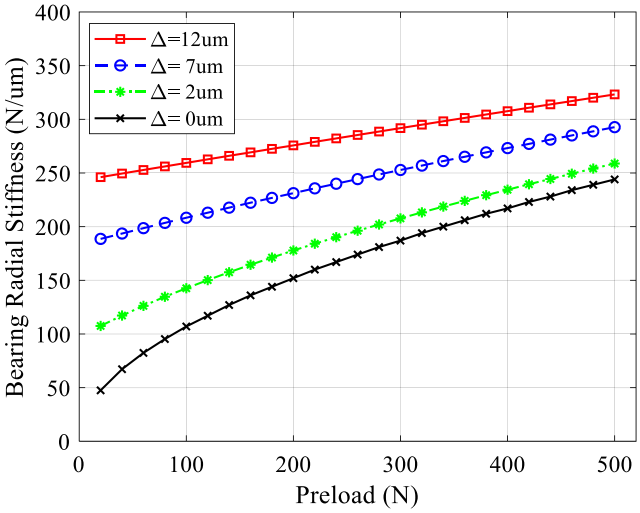

Fig. 4 Influence of interference fit values on bearing stiffness with different preloads

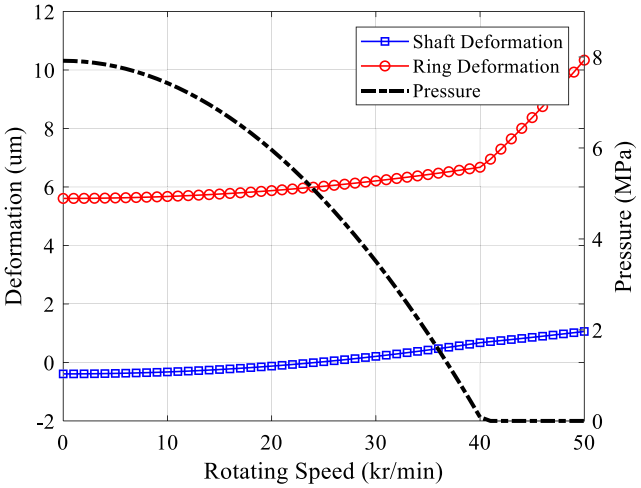

Fig. 6 Deformations of shaft and ring and the contact pressure at different rotating speed

3.2 Influence of interference fit on spindle-bearing system

In the spindle system, the existence of interference fit is essential to ensure the stability of the whole system. If the initial value of interference fit is too small, loosing or skidding between bearing inner ring and shaft will occur under high-speed conditions. This may result in the fretting wear, high-vibration of the shaft as well as eccentric of the spindle. Then, the rotating accuracy of the spindle system will drop sharply, and the vibration and noise will intensify at the same time. The loosing speed in this paper is defined as the maximum rotating speed of the spindle without skidding between bearing inner ring and shaft.

In order to avoid the arising of loosing during system operation, the quantitative relation between the initial values of interference fit and loosing speeds should be investigated. The derivations are already shown in the previous section, and the loosing will occur when the contact pressure between the bearing inner ring and shaft reduces to zero.

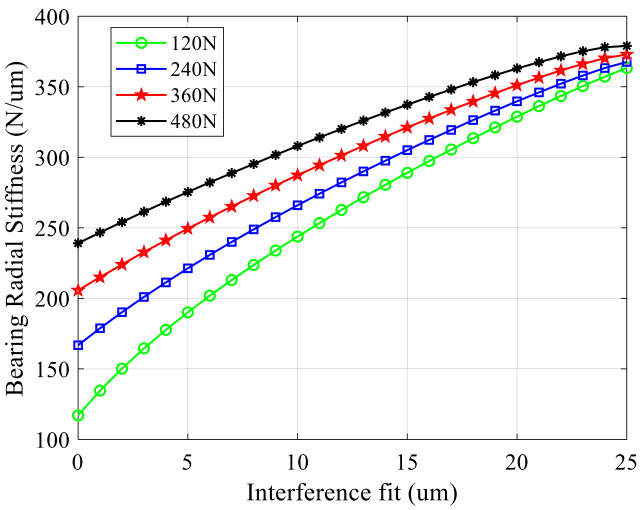

Fig. 5 Bearing stiffness under different interference fits

3.2.1 Shaft-bearing loosing speed under different values of initial interference fit

The bearing ring and shaft will deform under the actions of interference assembly and the centrifugal expansion. It is known that the bearing inner ring is quite thin, and its diameter is larger than the shaft. With the increasing of rotating speed, the expansion of bearing inner ring is much faster than the expansion of the shaft under the influence of centrifugal force.

Figure 6 shows the variation of the deformations of the matching bearing inner ring and the shaft, which is defined

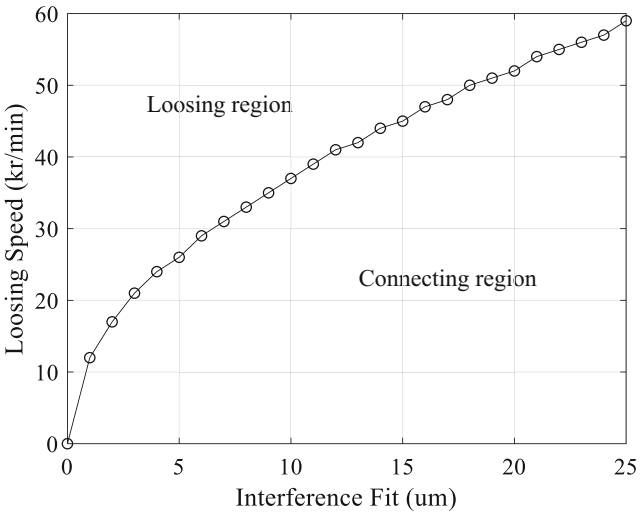

Fig. 7 Relationship between initial interference fit values and the system loosing speeds

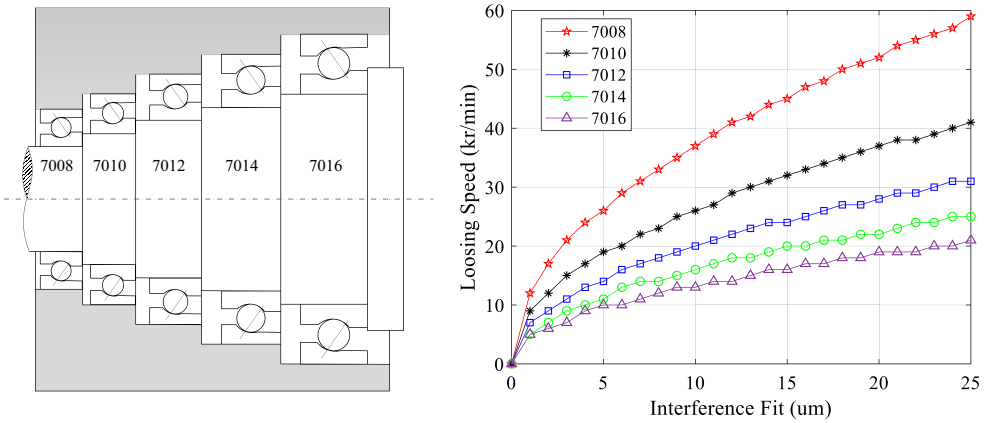

Fig. 8 The comparison of loosing speeds for different bearing sizes

as the diameter difference between the final state and nonassembly state. The value of the interference fit is specified as 12 μm in this case. Without loss of generality, the inner diameter of the ring is assumed as the nominal value, and the interference fit value is added on the diameter of the shaft. For the nonideal cases, there will be just a parallel transport on the curves if the diameters of both the inner ring and shaft are not the nominal values. The results show that with the increasing of rotating speed, the bearing inner ring and shaft will expand gradually.

Moreover, two regions, which are separated by a vertical dash-dotted line in Fig. 6, are clearly shown in the process of increasing system rotating speed. In the left-side region, the bearing inner ring and shaft are still under interconnection. Due to the interaction between the ring and shaft, which is also known as the boundary condition of the assembly based on the geometrical analysis, the value of the difference between bearing inner ring diameter and shaft outer diameter is a constant, i.e., the value of the initial interference fit. In the right-side region, the bearing inner ring and shaft lose contact as the value of difference between bearing inner ring diameter and shaft outer diameter is larger than the initial interference fit value. In this region, the interaction between the bearing inner ring and shaft does not exist and the two parts will expand separately under the influence of centrifugal force.

Similarly, the contact pressure between the bearing inner ring and shaft could also be used to describe the whole process, as shown in Fig. 6. In the left-side region, the contact pressure P is always present for the connection of the bearing inner ring and shaft even though the values are continuously declining for the inconsistent radial expansion of the assembly parts. In the right-side region, the contact pressure P reduced to zero for the disconnection between the bearing inner ring and shaft. The value of the rotating speed at the hinge is the loosing speed under a specific condition.

Figure 7 illustrates the relationship between initial interference fit values and the system loosing speeds. The results show that with the increasing of initial interference fit, the loosing speed will increase correspondingly. Based on this curve, it is known that the maximum of spindle speed should be less than the loosing speed in order to ensure the basic reliability of a spindle. This quantitative relationship is quite helpful on the practical design of the shaft-bearing system, especially for the high-speed spindles.

The interference fit is a quite important parameter in the design of spindle systems. Based on the proposed analytical model, much more simulations are conducted for spindle-bearing system using different bearing sizes or series.

The loosing speed under a specific interference fit will vary greatly with the changing of bearing sizes, which is obviously shown in the Fig. 8. Several cases with the bearing inner diameter changing in the range of 40~80 mm are investigated. The parameters of the bearing with different sizes are listed in Table 2. In order to ensure the comparability, the shaft is assumed as solid, as the schematic diagram shown in Fig. 8. The results show that the loosing speeds of shaft-bearing systems with a larger diameter are less sensitive to the initial interference fit, which means a tiny increment of the limiting rotational speed requires a big increment of the initial interference fit to ensure the reliability of the system connection.

Moreover, even for the bearings with the same inner diameters, their interference fits will also differ from each other if

Table 2 Bearing parameters of different sizes and series

Bearing numbers	Bearing bore diameter (mm)	Inner diameter of outer ring (mm)	Bearing width (mm)
71,808	40	44.1	7
71,908	40	48.5	12
7008	40	49.2	15
7208	40	66.7	18
7010	50	59.2	16
7012	60	70.8	18
7014	70	82.3	20
7016	80	93.9	22

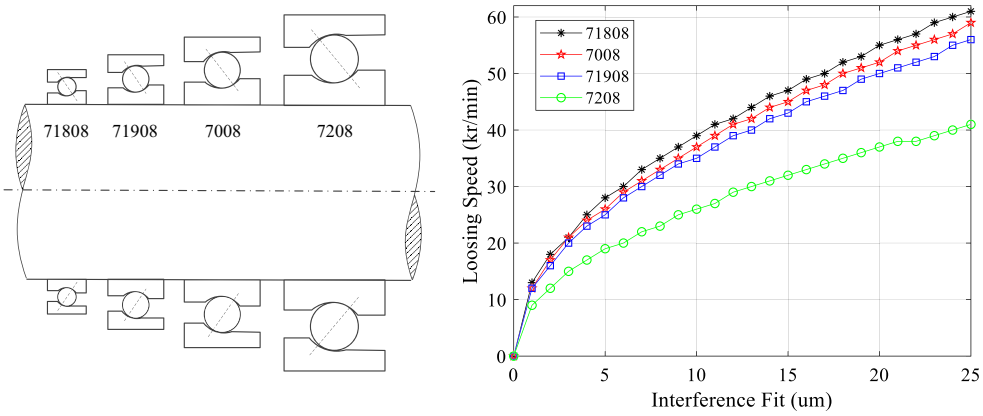

Fig. 9 The comparison of loosing speeds for different bearing series

they belong to different bearing series. The parameters of the bearing with different series are listed in Table 2. The curves in Fig. 9 represent the loosing speeds of shaft-bearing system with 718, 719, 70, and 72 *SKF*® bearing series, respectively. For these bearings, the inner bearing diameters are the same, 40 mm for this paper. However, the thickness of the bearing rings is different for different design purposes. The simulation results show that the thinner the bearing inner ring is, the higher the separation speed of the separation speed under the same interference fit values. So, for different bearing series, the interference fit values cannot be used mutually but should be designed specially in order to guarantee a perfect operating condition of the system.

3.2.2 Influence of interference fit on spindle static and dynamic characteristics

The bearing stiffness will be influenced by the bearing interference fit directly. For the integration of bearing model into the whole system, the spindle characteristics, such as the static stiffness, natural frequencies, and dynamic responses, will be further affected by the interference fit.

The variations of spindle static stiffness are shown in Fig. 10 under different initial interference fit values. Meanwhile, the influence of different bearing preloads is also taken into consideration. A remarkable increment is observed for the spindle stiffness when the initial value of interference fit increases under a specific preload value. The gradients of the spindle stiffness variation are greatly affected by the preload, and higher bearing preload will result in an obviously lower gradient of the spindle stiffness variation with the increasing of interference fit.

Besides, the related dynamic characteristics are also greatly influenced by the initial values of bearing interference fit. Based on the integrated analytical model, the natural frequencies of the spindle system are calculated under different interference fit values.

Figure 11 shows the variations of the first two natural frequencies of the spindle system with the changes of bearing initial interference fit values. The left graph gives the specific values of the natural frquencies under different conditions, and the right figure exhibits the spectra of the frequency response functions in detail. In these cases, the bearing preload is specified as 240 *N*. With the increasing of the initial values of interference fit, the system natural frequencies increase gradually. This phenomenon indicates the significant stiffen effects of the interference fit on the spindle system.

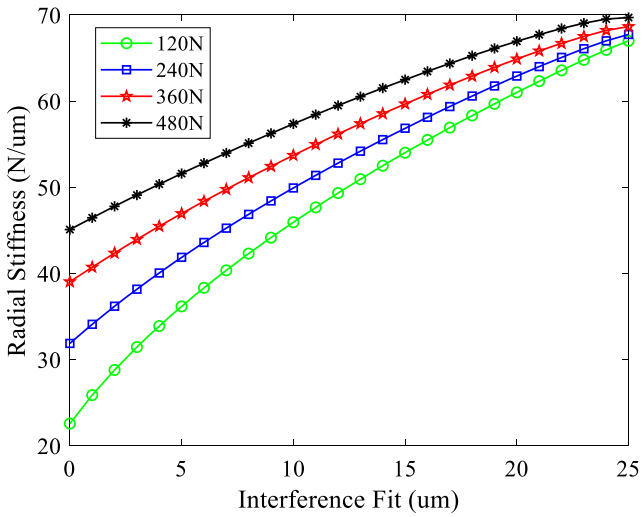

Fig. 10 Spindle radial stiffness with repsect to interference fit values under different preloads

4 Experimental verification

In order to verify the analytical model and the conclusions obtained from the corresponding simulation results, a specially designed spindle test rig is introduced to measure the spindle characteristics under different parameters. The static stiffness and the modal characteristics of the spindle are tested experimentally and the results are compared with the analytical simulations.

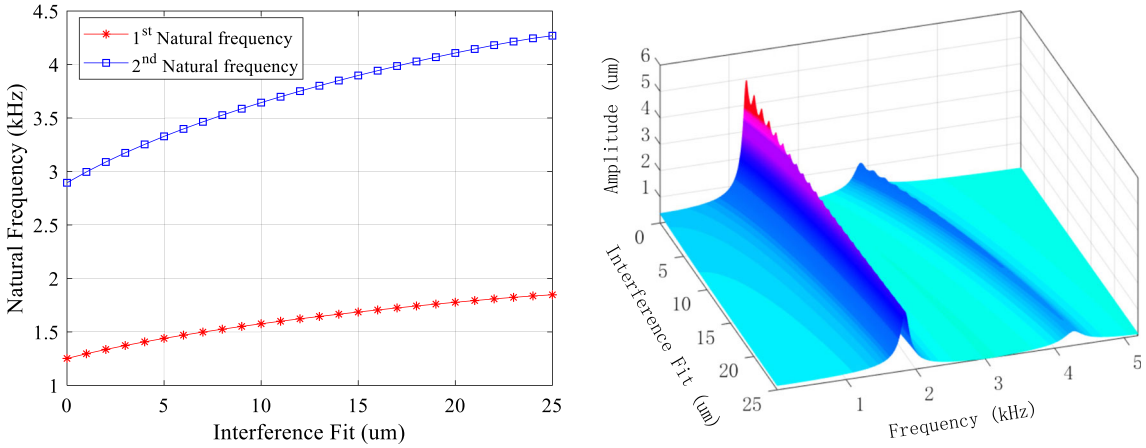

Fig. 11 The variation of the first two natural frequencies of the spindle system with repect to the interference fit values

The schematic of the spindle test rig has been shown in Sect. 3, the interference fit values between the shaft and bearing could be adjusted by adding thin slices between the surface of shaft and the bearing inner ring. The slice is made of steel with a thickness of 5 μm. By changing the interference fits of the shaft bearing system, the static and dynamic characteristics of the spindle in different situations could be tested. The original interference fit between the shaft and bearing is 2 μm, and the using of the thin slice could increase the interference fit to 12 μm.

Limited by the thickness of the slice, only two cases are included on the experiment, i.e., the cases with initial interference fit values 2 and 12 μm, respectively. In this spindle system, the bearing preload is designed as 240 N. For the difference of the testing purposes, the testing process of the spindle static stiffness and natural frequencies will be described separately.

4.1 Static stiffness of the spindle system

The spindle static stiffness is tested by measuring the radial displacements of the shaft front-end under different radial applied forces. A hydraulic cylinder, which is supported by an oil hydraulic pump with a maximum 5-t pressure, is utilized to provide variable forces in the vertical direction, and a force sensor is settled between the hydraulic cylinder and spindle to monitor the actual loading forces at a resolution of 1 N. Meanwhile, a micrometer gauge is fixed on the bearing

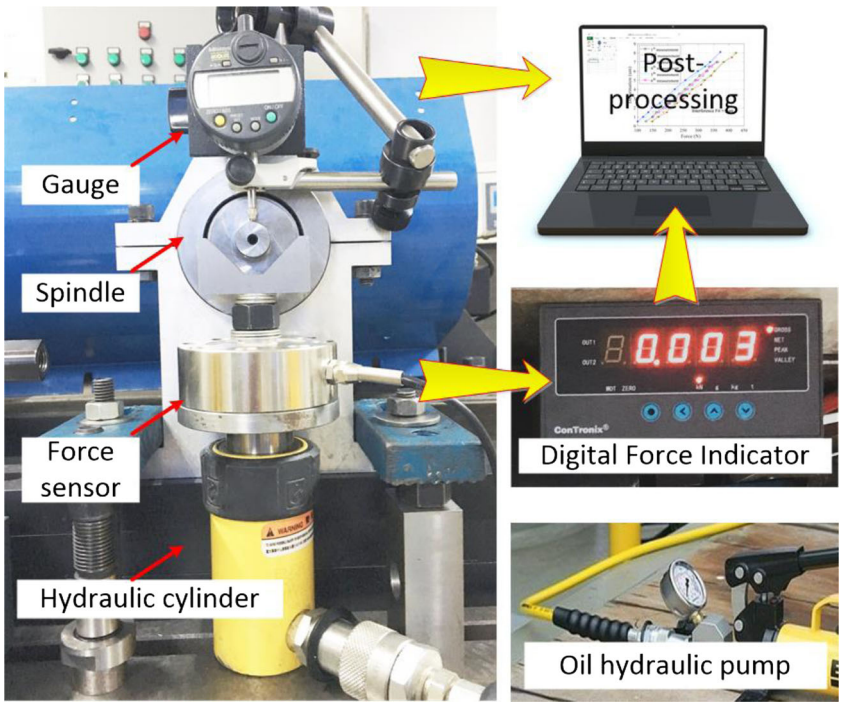

Fig. 12 Layout of the spindle static stiffness testing system

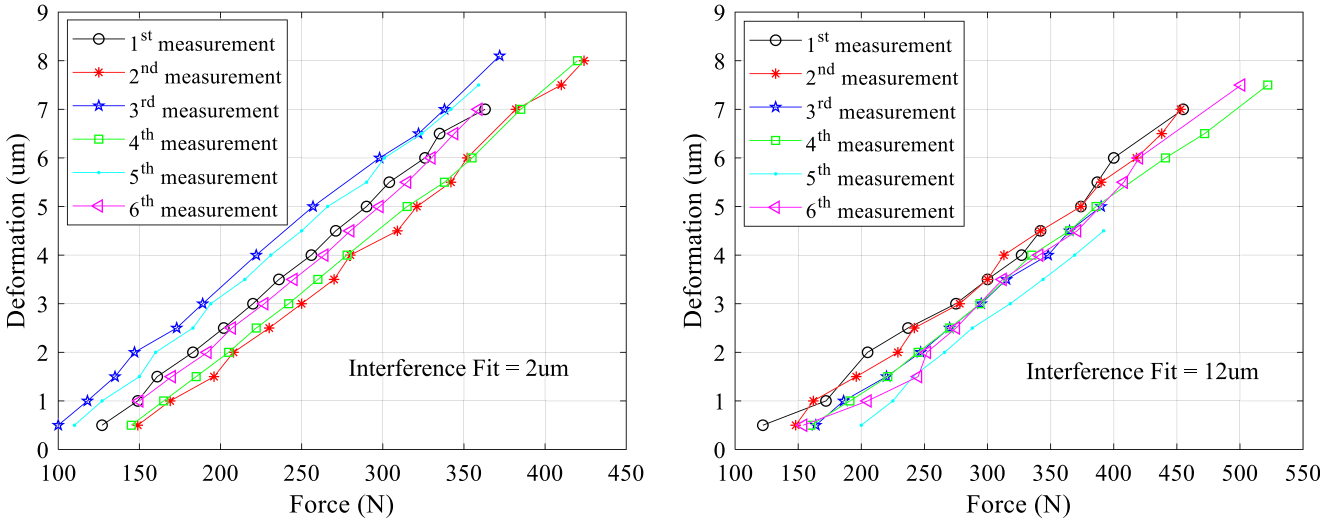

Fig. 13 Spindle stiffness under different bearing interference fits

housing for the recording of the relative displacement between shaft and housing. The detailed layout of the instruments is shown in Fig. 12.

The results of the spindle stiffness under different bearing interference fit values are shown in Fig. 13. For a specific value of interference fit, the measurements are repeated for six times. The results show that an approximate linear relationship shows up between the applied spindle radial force and the spindle reaction displacement in the radial direction, which means the spindle stiffness is a constant value under the loading range. For each specific measuring procedure, the spindle stiffness could be obtained by calculating the slope of the line, which could be constructed by linear data fit. The final testing spindle stiffness under a given interference fit value is the mean value of all the corresponding repetitive measurement results.

By extending the testing lines in the direction of decreasing force, we can find that the loading forces will not reduce to zero when the spindle radial deformations reach zero, i.e., the curves are not zero passage. This phenomenon is caused by the small clearance under the mating face of bearing outer ring and bearing housing.

The spindle stiffness is 35.7 N/μm for the interference fit value$\delta = 2$ μm and 49.2 N/μm for $\delta = 12$ μm. The testing results show an obvious increment in the spindle stiffness when a bigger bearing interference fit is applied, which agrees well with the analytical simulation results.

Table 3 Comparison of analytical and experimental spindle stiffness

Interference fit	Analytical	Experiment	Error
2 μm	36.2 N/μm	35.7 N/μm	− 1.40%
12 μm	52.8 N/μm	49.2 N/μm	− 7.32%

The analytical spindle stiffness under different interference fits is calculated in the previous section, and the comparison between analytical simulation and experimental results are shown in Table 3. A good agreement is shown according to the comparison. For the case with 12 μm initial interference fit, the error is much larger than the 2 μm case. The possible reason is that more mating faces will appear when the slice is used in the mating face between bearing inner ring and the shaft. The contact condition becomes more complex and is not as good as the case without using the slice, which means the using of slice reduced the contact reliability and connecting stiffness to some extent. However, the analytical model is ideal and without considering the new contacts introduced by the slice. This may be the primary factor that results in big difference between analytical and experiment results for 12 μm case.

4.2 Modal analysis: natural frequencies and frequency response function

The dynamic characteristics of the spindle system could be reflected by the system natural frequencies and frequency response function. In this paper, a modal testing equipment LMS Test. Lab, which is a kind of professional data acquisition and analysis system shown in Fig. 14, is used to capture the frequency response functions of the spindle with different interference fits. An impact hammer (sensitivity 0.21 mV/N) integrated with a force sensor (sensitivity 10 mV/g) is used to excite the spindle system in the shaft front-end with an impact load, and an acceleration sensor is employed to capture the system responses. In this process, both of the impact force and the acceleration signal acquisition directions are vertical.

The first two natural frequencies of the spindle system are obtained by the impact test and the comparison between

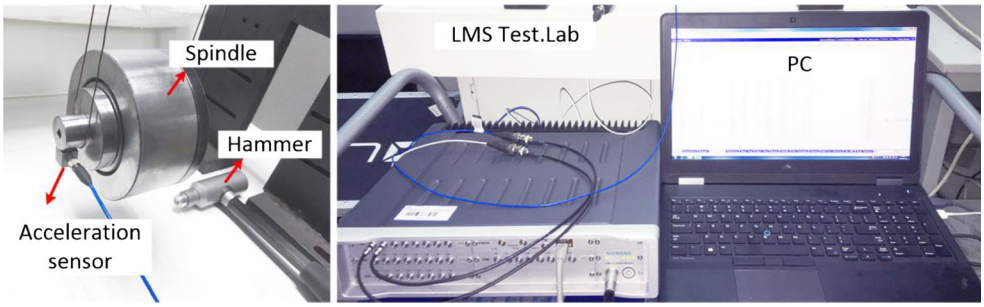

Fig. 14 Layout of the spindle modal testing system

analytical and experimental results are shown in Table 4. For both of the cases with different interference fits, the analytical and experimental results show good agreements.

The detailed frequency response functions of the spindle system under different bearing initial interference fit values are also calculated and compared, as shown in Fig. 15. Both of the FRFs are shown in the form of real and imag parts. For each graph in Fig. 15, an obvious shift shows up with the changing of interference fit values. The accuracy of the analytical model as well as the stiffen effects of the interference fit on spindle system are verified by the experiments.

Table 4 Comparison of analytical and experimental spindle natural frequencies

Interference fit	/	Analytical	Experiment	Error
2 μm	1st	1336 Hz	1384 Hz	3.47%
	2nd	3089 Hz	3268 Hz	5.48%
12 μm	1st	1623 Hz	1752 Hz	7.36%
	2nd	3751 Hz	3948 Hz	4.99%

5 Conclusions

In this paper, the influences of the bearing interference fit on bearing and spindle system are investigated using both analytical and experimental methods. By analyzing the internal geometric relationship among bearing parts, the influence of the interference fit is considered in the bearing stiffness model, and further coupled with the spindle model. The static and dynamic characteristics of the spindle system are simulated based on the proposed analytical model. In addition, the application of the analytical model in spindle stiffness and modal characteristic predictions is experimentally verified and the analytical and experimental results agree well with each other. The conclusions are summarized as follows:

The initial value of interference fit between bearing inner ring and shaft has great influence on bearing supporting stiffness. It is demonstrated that the low bearing preload cases are more sensitive to the change of interference fit values compared with high bearing preload ones due to the similar influence mechanism between the preload and interference fit.

The reliability of the connection between bearing inner ring and shaft is largely guaranteed by the interference fit. With the

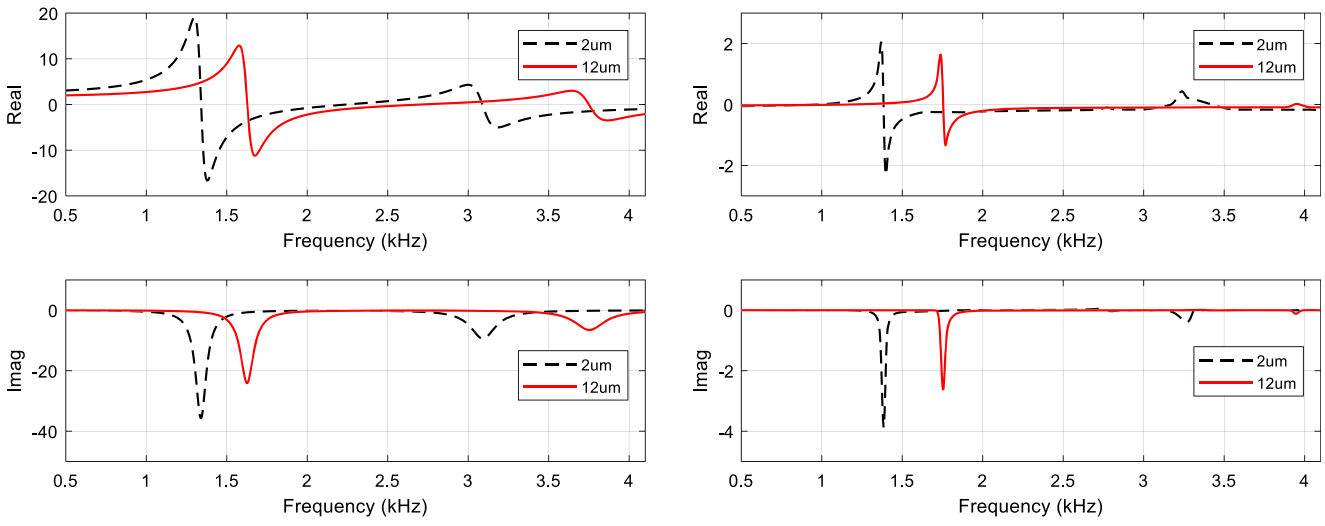

Fig. 15 Frequency response functions of the spindle system with different interference fit values. **a** Analytical results. **b** Experimental results

increase of the initial values of interference fit, the maximum limiting speed will increase correspondingly. Sufficient initial values of interference fit should be well designed quantificationally according to the bearing size as well as series.

The static and dynamic characteristics of spindle system, including the spindle static stiffness and natural frequencies, are also greatly affected by the initial value of bearing interference fit. The results show that the increasing of bearing interference fits will stiffen the spindle system and result in an obvious increment in the spindle stiffness and natural frequencies. The neglecting of this parameter will underestimate the whole system.

The analytical results calculated by the spindle-bearing model are experimentally verified using a specially designed spindle experiment rig. The good agreements between analytical predicted results and experimental data validated the accuracy of the proposed model in this paper.

For further research, the influence of clearance fits between bearing outer ring and housing should also be taken into consideration. Besides, the influence of thermodynamics is also nonnegligible and challengeable for spindle system under high speeds.

Funding information This research was supported by National Natural Science Foundation of China (Key Program): 51635010.

References

1. Abele E, Altintas Y, Brecher C (2010) Machine tool spindle units. CIRP Ann Manuf Technol 59(2):781–802
2. Lin CW, Lin YK, Chu CH (2013) Dynamic models and design of spindle-bearing systems of machine tools: a review. Int J Precis Eng Manuf 14(3):513–521
3. Chatterjee S (1996) Spindle deflections in high-speed machine tools - modelling and simulation. Int J Adv Manuf Technol 11(4): 232–239
4. Zverev IA, Eun IU, Chung WJ, Lee CM (2003) Simulation of spindle units running on rolling bearings. Int J Adv Manuf Technol 21(10–11):889–895
5. Jorgensen BR, Shin YC (1998) Dynamics of spindle-bearing systems at high speeds including cutting load effects. J Manuf Sci Eng Trans ASME 120(2):387–394
6. Chen JS, Hwang YW (2006) Centrifugal force induced dynamics of a motorized high-speed spindle. Int J Adv Manuf Technol 30(1–2):10–19
7. Cao Y, Altintas Y (2004) A general method for the modeling of spindle-bearing systems. J Mech Des Trans ASME 126(6):1089–1104
8. Cao Y, Altintas Y (2007) Modeling of spindle-bearing and machine tool systems for virtual simulation of milling operations. Int J Mach Tools Manuf 47(9):1342–1350
9. Jiang S, Zheng S (2010) Dynamic design of a high-speed motorized spindle-bearing system. J Mech Des 132(3):034501
10. Shaik JH, Srinivas J (2014) Influence of secondary factors of spindle geometry on the dynamic stability in end-milling operation. J Mech Des Vib 2(2):35–46
11. Cao H, Holkup T, Altintas Y (2011) A comparative study on the dynamics of high speed spindles with respect to different preload mechanisms. Int J Adv Manuf Technol 57(9):871–883
12. Wang B, Sun W, Xu K, Zhang J, Wen B (2014) The finite element modeling and stability prediction of high-speed spindle system dynamics with spindle-holder-tool joints. J Vibroeng 16(3):1188–1199
13. Xu C, Zhang J, Yu D, Wu Z, Feng P (2015) Dynamics prediction of spindle system using joint models of spindle tool holder and bearings. Proc Inst Mech Eng C J Mech Eng Sci 229(17):3084–3095
14. Özşahin O, Altintas Y (2015) Prediction of frequency response function (FRF) of asymmetric tools from the analytical coupling of spindle and beam models of holder and tool. Int J Mach Tools Manuf 92:31–40
15. Ertürk A, Özgüven HN, Budak E (2006) Analytical modeling of spindle–tool dynamics on machine tools using Timoshenko beam model and receptance coupling for the prediction of tool point FRF. Int J Mach Tools Manuf 46(15):1901–1912
16. Ertürk A, Özgüven HN, Budak E (2007) Effect analysis of bearing and interface dynamics on tool point FRF for chatter stability in machine tools by using a new analytical model for spindle–tool assemblies. Int J Mach Tools Manuf 47(1):23–32
17. Yang Y, Wan M, Ma YC, Zhang WH (2018) A new method using double distributed joint interface model for three-dimensional dynamics prediction of spindle-holder-tool system. Int J Adv Manuf Technol 95(5–8):2729–2745
18. Hung JP, Yuan L, Luo TL, Su HC (2013) Analysis of the machining stability of a milling machine considering the effect of machine frame structure and spindle bearings: experimental and finite element approaches. Int J Adv Manuf Technol 68(9–12):2393–2405
19. Zivkovic A, Zeljkovic M, Tabakovic S, Milojevic Z (2015) Mathematical modeling and experimental testing of high-speed spindle behavior. Int J Adv Manuf Technol 77(5–8):1071–1086
20. Li H, Shin YC (2004) Integrated dynamic thermomechanical modeling of high speed spindles, part 1: model development. J Manuf Sci Eng 126(1):148–158
21. Li H, Shin YC (2008) Integration of thermo-dynamic spindle and machining simulation models for a digital machining system. Int J Adv Manuf Technol 40(7–8):648–661
22. Lin CW, Tu JF, Kamman J (2003) An integrated thermo-mechanical-dynamic model to characterize motorized machine tool spindles during very high speed rotation. Int J Mach Tools Manuf 43(10):1035–1050
23. Lin CW, Tu JF (2007) Model-based design of motorized spindle systems to improve dynamic performance at high speeds. J Manuf Process 9(2):94–108
24. Lin CW (2011) An application of Taguchi method on the high-speed motorized spindle system design. Proc Inst Mech Eng C J Mech Eng Sci 225(9):2198–2205
25. Holkup T, Cao H, Kolář P, Altintas Y, Zelený J (2010) Thermo-mechanical model of spindles. CIRP Ann Manuf Technol 59(1): 365–368
26. Liu J, Chen X (2014) Dynamic design for motorized spindles based on an integrated model. Int J Adv Manuf Technol 71(9–12):1961–1974
27. El-Saeidy FMA (2011) Time-varying total stiffness matrix of a rigid machine spindle-angular contact ball bearings assembly: theory and analytical/experimental verifications. Shock Vib 18(5):641–670
28. Li X, Li H, Zhang Y, Hong J (2016) Investigation of non-uniform preload on the static and rotational performances for spindle bearing system. Int J Mach Tools Manuf 106:11–21

29. Jones AB (1960) A general theory for elastically constrained ball and radial roller bearings under arbitrary load and speed conditions. J Basic Eng 82(2):309–320
30. Harris TA, Mindel MH (1973) Rolling element bearing dynamics. Wear 23(3):311–337
31. Xi S, Cao H, Chen X, Niu L (2017) A dynamic modeling approach for spindle bearing system supported by both angular contact ball bearing and floating displacement bearing. J Manuf Sci Eng 140(2): 021014–021016
32. Yan K, Hong J, Zhang J, Mi W, Wu W (2016) Thermal-deformation coupling in thermal network for transient analysis of spindle-bearing system. Int J Therm Sci 104:1–12
33. Cao L, Sadeghi F, Stacke L-E (2017) A combined EFEM–discrete element method dynamic model of rotor–bearing–housing system. J Tribol 139(6):061102–061110
34. Zhang J, Fang B, Zhu Y, Hong J (2017) A comparative study and stiffness analysis of angular contact ball bearings under different preload mechanisms. Mech Mach Theory 115:1–17
35. Cao Y (2006) Modeling of high-speed machine-tool spindle systems. Dissertation Abstracts International, Volume: 67-12, Section: B, p 7325